High-Energy Photon Splitting in the Electric Fields of Heavy Atoms

R.N. Lee, A.I. Milstein, V.M. Strakhovenko

Budker Institute of Nuclear Physics, 630090 Novosibirsk, Russia

Abstract

Various differential cross sections of high-energy photon splitting in the electric fields of heavy atoms are calculated exactly in the parameter $Z\alpha$. The consideration is based on the quasiclassical approach applicable for small angles between all photon momenta. The expressions obtained are valid for arbitrary transverse momenta of final photons . The detailed investigation of the process is performed taking into account the effect of screening . The exact cross section turns out to be noticeably smaller than the result obtained in the Born approximation.

1 Introduction

The first successful observation of high-energy photon splitting in the electric fields of atoms has been recently performed in the Budker Institute of Nuclear Physics. A crystal of $Bi_4Ge_3O_{12}$ has been used as a target. At the present time, the data processing is almost completed and preliminary results are published in [1]. Theoretical and experimental investigation of this nonlinear QED process is important as a new test of QED in strong external fields. It also gives a possibility to understand the role and the structure of higher orders of the perturbation theory with respect to the external field since, as is shown in the present paper, the exact in $Z\alpha$ cross section ($Z|e|$ is the nucleus charge, $\alpha = e^2/4\pi = 1/137$ is the fine-structure constant, e is the electron charge) differs essentially from that obtained in the Born approximation, i.e. in the lowest order in $Z\alpha$.

The cross section of photon splitting was found in [2, 3] in the Born approximation. In the same approximation, an essentially simpler form of the cross section was obtained in [4] with the help of the Weizsäcker-Williams method providing the logarithmic accuracy. Using the analytical results of [2, 3], the cross section of the photon splitting was investigated numerically in [5, 6].

The Coulomb corrections represent the difference between the exact (with exact account for an external field) cross section of the process and the result obtained in the Born approximation. Basing on our experience concerning Delbrück scattering, we expected a measureable effect in the photon splitting too. In recent papers [7, 8] general formulae for the high-energy photon splitting amplitudes have been derived exactly in $Z\alpha$ for small angles f_2 and f_3 between the momenta $\mathbf{k}_2$, $\mathbf{k}_3$ of the final photons and the momentum $\mathbf{k}_1$ of the initial one ($\omega_i = |\mathbf{k}_i| \gg m$, m is the electron mass). It is the region of small angles, which makes the main contribution to the total cross section of the process. Additionally, small angles and high photon energies allow one to apply the quasiclassical approach, developed in [9, 10] at the consideration of Delbrück scattering (see recent review [11]). This approach is based on the use of the quasiclassical Green function for the Dirac equation in the electric field of an atom, which is equivalent to a summation for all orders of the perturbation theory with respect to the external field. The quasiclassical approach greatly simplifies the calculation of amplitudes.

First theoretical results concerning Coulomb corrections in the process of photon splitting were obtained in[8] for large transverse momenta of the final photons as compared to the electron mass: $|\mathbf{k}_{2\perp}| = \omega_2 f_2 \gg m$ and $|\mathbf{k}_{3\perp}| = \omega_3 f_3 \gg m$. It turned out that in this kinematical region the Coulomb corrections lead to the significant decrease of the cross section. They become noticeable starting from relatively small Z and reach several tens per cent for heavy atoms.

In the present paper we discuss the exact cross section of the process in the limit of high energy of the initial photon for arbitrary transverse momenta of the final photons. We examine numerically the role of the Coulomb corrections in various differential cross sections. We discuss the case of a pure Coulomb field as well as the effect of screening.

2 Amplitudes of the process

As was shown in [7, 8], it is convenient to present the initial expression for the photon splitting amplitude in the form containing the Green functions $D(x,x')$ of the "squared" Dirac equation:

$$D(x,x') = \langle x|1/(\hat{\mathcal{P}}^2 - m^2 + i0)|x'\rangle \ ,$$

where $\hat{\mathcal{P}} = \gamma^\mu(i\partial_\mu - g_{\mu 0}U(r))$, $U(r)$ is the potential energy of an electron in an external field, γ^μ are the Dirac matrices. Then the amplitude M is splitted into a sum of the perturbation-theory diagrams, containing either three or two Green functions $D(x,x')$: $M = M^{(3)} + M^{(2)}$. The term $M^{(3)}$ is given by

$$\begin{aligned} M^{(3)} &= \frac{i}{2}e^3 \int \frac{d\varepsilon}{2\pi} \int d\mathbf{r}_1 d\mathbf{r}_2 d\mathbf{r}_3 \exp[i(\mathbf{k}_1\mathbf{r}_1 - \mathbf{k}_2\mathbf{r}_2 - \mathbf{k}_3\mathbf{r}_3)] \times \\ &\mathrm{Tr}\Big\{[(-\hat{e}_1\hat{k}_1 - 2\mathbf{e}_1\mathbf{p})D(\mathbf{r}_1,\mathbf{r}_2\,|\varepsilon-\omega_2)][(\hat{e}_2^*\hat{k}_2 - 2\mathbf{e}_2^*\mathbf{p})D(\mathbf{r}_2,\mathbf{r}_3\,|\varepsilon)] \times \\ &[(\hat{e}_3^*\hat{k}_3 - 2\mathbf{e}_3^*\mathbf{p})D(\mathbf{r}_3,\mathbf{r}_1\,|\varepsilon+\omega_3)]\Big\} + (k_2^\mu \leftrightarrow k_3^\mu\,,\ \mathbf{e}_2 \leftrightarrow \mathbf{e}_3)\,. \end{aligned} \tag{1}$$

Here e_1^μ and $e_{2,3}^\mu$ are the polarization vectors of the initial and final photons, $\hat{e} = e^\mu\gamma_\mu = -\mathbf{e}\boldsymbol{\gamma}$, and the operator $\mathbf{p} = -i\boldsymbol{\nabla}$ differentiates the Green function D with respect to its first argument. The term $M^{(2)}$ reads

$$\begin{aligned} M^{(2)} &= ie^3 \int \frac{d\varepsilon}{2\pi} \int d\mathbf{r}_1 d\mathbf{r}_2\, \mathrm{Tr}\Big\{\exp[i(\mathbf{k}_1\mathbf{r}_1 - \mathbf{k}_2\mathbf{r}_2 - \mathbf{k}_3\mathbf{r}_2)]\,\mathbf{e}_2^*\mathbf{e}_3^* \times \\ &[(-\hat{e}_1\hat{k}_1 - 2\mathbf{e}_1\mathbf{p})D(\mathbf{r}_1,\mathbf{r}_2\,|\varepsilon-\omega_1)]\,D(\mathbf{r}_2,\mathbf{r}_1\,|\varepsilon)] \\ &+\Big[\exp[i(\mathbf{k}_1\mathbf{r}_1 - \mathbf{k}_2\mathbf{r}_2 - \mathbf{k}_3\mathbf{r}_1)]\,\mathbf{e}_1\mathbf{e}_3^* \times \\ &D(\mathbf{r}_1,\mathbf{r}_2\,|\varepsilon-\omega_2)]\,[(\hat{e}_2^*\hat{k}_2 - 2\mathbf{e}_2^*\mathbf{p})D(\mathbf{r}_2,\mathbf{r}_1\,|\varepsilon)] + (k_2^\mu \leftrightarrow k_3^\mu\,,\ \mathbf{e}_2 \leftrightarrow \mathbf{e}_3)\Big]\Big\}\,. \end{aligned} \tag{2}$$

As was pointed out in [7], the effect of screening is important only for the lowest (Born) approximation in $Z\alpha$. Therefore, we start from the case of a pure Coulomb potential $U(r) = -Z\alpha/r$ and then multiply the Born contribution to the amplitude by the atomic form factor to take the effect of screening into account.

It is convenient to perform the calculations in terms of the helicity amplitudes
$M_{\lambda_1\lambda_2\lambda_3}(\mathbf{k}_1,\mathbf{k}_2,\mathbf{k}_3)$. We direct the z axis along $\mathbf{k}_1$ and introduce the vectors $\mathbf{f}_2=\mathbf{k}_{2\perp}/\omega_2$ and $\mathbf{f}_3=\mathbf{k}_{3\perp}/\omega_3$ ($|\mathbf{f}_{2,3}|\ll 1$). The z component of the polarization vectors $\mathbf{e}_i$ can be eliminated owing to the relation $\mathbf{e}_i\mathbf{k}_i=0$ which leads to $e_z=-\mathbf{e}_\perp\mathbf{k}_\perp/\omega$. After that within the small-angle approximation one can neglect the difference between the vectors $(\mathbf{e}_{2,3})_\perp$ and the polarization vectors of photons, propagating along the z axis and having the same helicities. Therefore, the amplitudes $M_{\lambda_1\lambda_2\lambda_3}(\mathbf{k}_1,\mathbf{k}_2,\mathbf{k}_3)$ contain only the transverse polarization vectors $\mathbf{e}$ and $\mathbf{e}^*$, corresponding to the positive and negative helicities, respectively. It is sufficient to calculate three amplitudes, for instance, $M_{+--}(\mathbf{k}_1,\mathbf{k}_2,\mathbf{k}_3)$, $M_{+++}(\mathbf{k}_1,\mathbf{k}_2,\mathbf{k}_3)$ and $M_{++-}(\mathbf{k}_1,\mathbf{k}_2,\mathbf{k}_3)$. Other amplitudes can be obtained by the substitution

$$M_{+-+}(\mathbf{k}_1,\mathbf{k}_2,\mathbf{k}_3)=M_{++-}(\mathbf{k}_1,\mathbf{k}_3,\mathbf{k}_2)\,,$$

$$M_{-\lambda_2\lambda_3}(\mathbf{k}_1,\mathbf{k}_2,\mathbf{k}_3)=M_{+\Lambda_2\Lambda_3}(\mathbf{k}_1,\mathbf{k}_2,\mathbf{k}_3)\,(\mathbf{e}\leftrightarrow\mathbf{e}^*)\,,$$

where Λ denotes the helicity opposite to λ.

In [12] we obtained the following expressions for the helicity amplitudes of photon splitting

$$\begin{aligned}
M_{+--} &= N\!\int\! d\mathbf{x}\,(\mathbf{eG})\!\int_0^{\omega_2}\!\frac{d\varepsilon}{A}\kappa_2\left[-\mathbf{ea}\left(\frac{\varepsilon}{\mathbf{e}^*\mathbf{f}_3}+\frac{\kappa_3}{\mathbf{e}^*\mathbf{f}_{23}}\right)\right.\\
&\left.+\,m^2\omega_3\kappa_2\left(\frac{\kappa_3\,\mathbf{ef}_{23}}{\omega_1\mathcal{D}_1\mathbf{e}^*\mathbf{f}_{23}}-\frac{\varepsilon\,\mathbf{ef}_3}{\omega_2\mathcal{D}_3\mathbf{e}^*\mathbf{f}_3}\right)\right]+\left(\begin{array}{c}\omega_2\leftrightarrow\omega_3\\ \mathbf{f}_2\leftrightarrow\mathbf{f}_3\end{array}\right),
\end{aligned}\tag{3}$$

$$\begin{aligned}
M_{+++} &= N\!\int\! d\mathbf{x}\!\int_0^{\omega_2}\frac{d\varepsilon}{2A}\left[\frac{\mathbf{eG}\,(\kappa_2^2+\kappa_3^2)}{\mathbf{ef}_{23}}\left(\mathbf{e}^*\mathbf{a}-\frac{m^2\omega_3\kappa_2\,\mathbf{e}^*\mathbf{f}_{23}}{\omega_1\mathcal{D}_1}\right)+\right.\\
&\frac{\omega_1\omega_3\kappa_2G_1\mathbf{e}^*\,(\mathbf{a}+\mathbf{f}_{23}\omega_2\kappa_3/\omega_1)}{\mathcal{D}_1}+\frac{\omega_3\kappa_2\,\mathbf{e}^*\mathbf{G}}{\omega_2\mathcal{D}_3}[\varepsilon\omega_3A+2\varepsilon\left(\kappa_2^2+\kappa_3^2\right)(\mathbf{e}^*\mathbf{f}_3)\,(\mathbf{ea})+\\
&\left.m^2(2\varepsilon\kappa_2-\omega_1\omega_2)]-\frac{\omega_1\omega_3\kappa_2G_1\,\mathbf{e}^*\mathbf{c}}{\mathcal{D}_3}\right]+\left(\begin{array}{c}\omega_2\leftrightarrow\omega_3\\ \mathbf{f}_2\leftrightarrow\mathbf{f}_3\end{array}\right),
\end{aligned}$$

$$\begin{aligned}
M_{++-} &= N\int d\mathbf{x}\left\{\int_0^{\omega_2}\frac{d\varepsilon}{2A}\left[\frac{\kappa_2\omega_3\,\mathbf{eG}}{\omega_1\mathcal{D}_1}[\kappa_3\left(\kappa_2-\varepsilon\right)A\right.\right.\\
&-2\kappa_3\left(\kappa_2^2+\varepsilon^2\right)(\mathbf{ef}_{23})\,(\mathbf{e}^*\mathbf{a})+m^2\left(\omega_1\omega_2-2\kappa_2\kappa_3\right)]+\frac{\kappa_2\omega_2\omega_3G_1\,\mathbf{eb}}{\mathcal{D}_1}
\end{aligned}$$

$$+\frac{\left(\kappa_2^2+\varepsilon^2\right)\mathbf{e}^*\mathbf{G}}{\mathbf{e}^*\mathbf{f}_3}\left(\mathbf{ea}+\frac{m^2\omega_3\kappa_2\,\mathbf{ef}_3}{\omega_2\mathcal{D}_3}\right)-\frac{\omega_2\omega_3\kappa_2G_1\mathbf{e}\left(\mathbf{a}+\mathbf{f}_3\omega_1\varepsilon/\omega_2\right)}{\mathcal{D}_3}\Bigg]$$

$$+\int_{-\omega_3}^{0}d\varepsilon\frac{\omega_2\kappa_3}{2B}\left[\frac{\mathbf{eG}}{\omega_1\mathcal{D}_1}[-\left(\kappa_2^2+\varepsilon\kappa_3\right)B+2\kappa_3\left(\kappa_2^2+\varepsilon^2\right)\left(\mathbf{e}^*\mathbf{f}_{23}\right)(\mathbf{eb})\right.$$

$$+m^2\left(\omega_1\omega_2-2\kappa_2\kappa_3\right)]+\frac{\omega_2G_1\,\mathbf{eb}}{\mathcal{D}_1}+\frac{\mathbf{eG}}{\omega_3\mathcal{D}_2}[-\omega_2\kappa_3B$$

$$\left.\left.+\;2\kappa_3\left(\kappa_2^2+\varepsilon^2\right)\left(\mathbf{e}^*\mathbf{f}_2\right)(\mathbf{eb})+m^2\left(\omega_2\omega_3-2\varepsilon\kappa_3\right)]+\frac{\omega_2G_1\,\mathbf{eb}}{\mathcal{D}_2}\right]\right\}\;,$$

where the following notation is used

$$\mathbf{a}=\mathbf{x}-\boldsymbol{\Delta}/2+\kappa_2\mathbf{f}_2\quad,\quad\mathbf{b}=\mathbf{x}+\boldsymbol{\Delta}/2-\kappa_3\mathbf{f}_3\quad,\quad\mathbf{c}=\mathbf{x}+\boldsymbol{\Delta}/2-\varepsilon\mathbf{f}_{23}\,,\qquad(4)$$

$$N=\frac{8e^3Z\alpha}{\pi^2\Delta^2\omega_1\omega_2\omega_3}\quad,\quad A=m^2+\mathbf{a}^2\quad,\quad B=m^2+\mathbf{b}^2\quad,$$

$$\mathcal{D}_1=\left(\mathbf{x}+\frac{\kappa_2-\kappa_3}{2\omega_1}\boldsymbol{\Delta}\right)^2-\frac{\omega_2\omega_3\kappa_2\kappa_3}{\omega_1^2}\mathbf{f}_{23}^2-i0\quad,$$

$$\mathcal{D}_2=\left(\mathbf{x}-\frac{\kappa_3+\epsilon}{2\omega_3}\boldsymbol{\Delta}\right)^2-\frac{\omega_1\omega_2\kappa_3\epsilon}{\omega_3^2}\mathbf{f}_2^2\quad,$$

$$\mathcal{D}_3=\left(\mathbf{x}+\frac{\kappa_2-\epsilon}{2\omega_2}\boldsymbol{\Delta}\right)^2+\frac{\omega_1\omega_3\kappa_2\epsilon}{\omega_2^2}\mathbf{f}_3^2\quad,$$

$$\mathbf{G}=\cos\,\tau\,\left(\frac{\mathbf{x}+\boldsymbol{\Delta}/2}{c_+}-\frac{\mathbf{x}-\boldsymbol{\Delta}/2}{c_-}\right)\mathcal{F}_1+\sin\,\tau\,\left(\frac{\mathbf{x}+\boldsymbol{\Delta}/2}{c_+}+\frac{\mathbf{x}-\boldsymbol{\Delta}/2}{c_-}\right)\mathcal{F}_2\;,$$

$$G_1=m^2\cos\,\tau\,\left(\frac{1}{c_-}-\frac{1}{c_+}\right)\mathcal{F}_1+\sin\,\tau\,\left(1-\frac{m^2}{c_+}-\frac{m^2}{c_-}\right)\mathcal{F}_2\,.$$

Here

$$c_\pm=m^2+\left(\mathbf{x}\pm\boldsymbol{\Delta}/2\right)^2\;,\;a=\sqrt{\frac{m^2\boldsymbol{\Delta}^2}{c_+c_-}}\;,\;\tau=Z\alpha\ln\left(\frac{c_+}{c_-}\right)\;,$$

and the functions $\mathcal{F}_1$ and $\mathcal{F}_2$ are equal to

$$\mathcal{F}_1=\int_0^\infty\frac{dx}{\left(1+x^2\right)^{3/2}}\cos\left(2Z\alpha\,\mathrm{arcsinh}(ax)\right)\;,\qquad(5)$$

$$\mathcal{F}_2=\int_0^\infty\frac{dx}{\left(1+x^2\right)^{3/2}}\sin\left(2Z\alpha\,\mathrm{arcsinh}(ax)\right)\frac{ax}{\sqrt{1+a^2x^2}}$$

As was pointed out in [7], the quantity Δ^2 in the coefficient N should be interpreted as the squared total momentum transfer:

$$\Delta^2 = (\mathbf{k}_2 + \mathbf{k}_3 - \mathbf{k}_1)^2 = \boldsymbol{\Delta}^2 + \Delta_z^2 = (\mathbf{k}_{2\perp} + \mathbf{k}_{3\perp})^2 + \frac{1}{4}\left(\frac{\mathbf{k}_{2\perp}{}^2}{\omega_2} + \frac{\mathbf{k}_{3\perp}{}^2}{\omega_3}\right)^2 . \quad (6)$$

Since the functions $\mathbf{G}$ and G_1 are independent of the energy ε, the integrands in (3) are rational functions of ε, where all the denominators are quadratic forms of this variable. Therefore, the integrals over ε can be expressed via elementary functions. Resulting formulae being rather cumbersome are not presented here explicitly. Performing the integration over ε in (3), we obtain in fact a twofold integral over $\mathbf{x}$ for the amplitude of photon splitting since for a given $Z\alpha$, the functions $\mathcal{F}_1$ and $\mathcal{F}_2$ (see (5)) can be tabulated separately. In the limit $m \to 0$ the amplitudes (3) coincides with those obtained previously in [8]. Additionally, it has been checked numerically that in the limit $Z\alpha \to 0$ our results (3) agree with those, obtained in [5, 6] in the Born approximation.

3 Cross section

In the small-angle approximation ($|\mathbf{f}_2|, |\mathbf{f}_3| \ll 1$) the cross section of photon splitting has the form

$$d\sigma = |M|^2 \frac{dx\, d\mathbf{k}_{2\perp}\, d\mathbf{k}_{3\perp}}{2^8 \pi^5 \omega_1^2 x(1-x)} \quad , \quad (7)$$

where $x = \omega_2/\omega_1$, so that $\omega_3 = \omega_1(1-x)$. In the present paper a screened Coulomb potential is used in all the calculations. As was explained above, to take screening into account, the lowest in $Z\alpha$ (Born) part of the amplitude should be multiplied by the atomic form factor. The Molière representation [13] for this form factor reads

$$1 - F(\Delta^2) = \Delta^2 \sum_{i=1}^{3} \frac{\alpha_i}{\Delta^2 + \beta_i^2} , \quad (8)$$

where

$$\alpha_1 = 0.1, \quad \alpha_2 = 0.55, \quad \alpha_3 = 0.35, \quad \beta_i = \beta_0 b_i, \quad (9)$$

$$b_1 = 6, \quad b_2 = 1.2, \quad b_3 = 0.3, \quad \beta_0 = mZ^{1/3}/121.$$

To illustrate a magnitude of the Coulomb corrections, the exact and Born differential cross sections $d\sigma/dxd\mathbf{k}_{2\perp}d\mathbf{k}_{3\perp}$ are plotted in Fig.1 depending on $|k_{2\perp}|/m$ for $|\mathbf{k}_{3\perp}| = 2m$ and the azimuth angle (the angle between the vectors $\mathbf{k}_{2\perp}$ and $\mathbf{k}_{3\perp}$) $\phi = 0, \pi$. The calculations were performed for a screened Coulomb potential at $x = 0.1$, $\omega_1 = 1$GeV. The value $Z = 83$ (bismuth) was chosen since bismuth atoms determine the cross section of photon splitting in the experiment [1]. A wide peak for azimuth angle $\phi = \pi$ is due to small momentum transfer Δ. There is a narrow notch in the middle of this peak (at $|k_{2\perp}|/m = 2$) where the condition $\mathbf{\Delta}_\perp = \mathbf{k}_{2\perp} + \mathbf{k}_{3\perp} = 0$ is fulfilled. The width of the notch is about $\max(\Delta_z/m, \beta_0/m)$. Recall that Δ_z is the longitudinal component of the momentum transfer defined by (6), and β_0 (9) characterizes the effect of screening. In our example β_0 is larger than Δ_z , so the width of the notch is roughly $\beta_0/m = 3.6 \cdot 10^{-2}$. Let us note that for $\omega_1 \gg m$ the differential cross section, expressed in terms of $\mathbf{k}_{2\perp}$, $\mathbf{k}_{3\perp}$, x and ω_1 depends on the energy ω_1 only via Δ_z. Due to this, the differential cross section is independent of ω_1 outside the notch vicinity. The behavior of the cross section at small Δ is determined by the Born amplitude which is proportional to $1/\Delta$ in this case. That is why the exact and Born cross sections coincide within peak region. Outside this region the Coulomb corrections essentially modify the cross section. The points of discontinuous slope on the curves in Fig.1 are related to the threshold conditions for real electron-positron pair production by two photons with the momenta $\mathbf{k}_2$ and $\mathbf{k}_3$:

$$(k_2 + k_3)^2 = \omega_2\omega_3\mathbf{f}_{23}^2 = 4m^2 \ . \tag{10}$$

In Figs. 2-4 the differential cross section $m^2\sigma_0^{-1}d\sigma/dx\, d\mathbf{k}_{2\perp}$ is shown depending on $k_{2\perp}/m$ for a screened Coulomb potential at $\omega_1/m = 1000$, $Z = 83$ and different x,

$$\sigma_0 = \frac{\alpha^3(Z\alpha)^2}{4\pi^2m^2} = 0.782 \cdot 10^{-9}\, Z^2 \text{ b} \ .$$

Solid curves represent the exact cross sections, and the dashed curves give the Born results. The cross section exhibits a thresholdlike behavior in the vicinity of the point $k_{2\perp} = k_{th} = 2\sqrt{x(1-x)}m$, where both conditions $\mathbf{\Delta} = \mathbf{k}_{2\perp} + \mathbf{k}_{3\perp} = 0$ and (10) hold. Under these conditions the peak in the cross section $d\sigma/dxd\mathbf{k}_{2\perp}d\mathbf{k}_{3\perp}$ seats on the boundary of the kinematic region where real electron-positron pair production by two photons with the momenta $\mathbf{k}_2$ and $\mathbf{k}_3$ is possible. The cross sections $d\sigma/dx\,d\mathbf{k}_{2\perp}$ drop rapidly for $k_{2\perp} \gg m$ ($\propto 1/k_2^4$). The dotted curves in Figs. 2-4 show the difference between the Born and exact cross sections, i.e. they give the Coulomb corrections taken with the opposite sign. Again, as is seen from Figs.2-4, the Coulomb corrections to the cross section integrated over $\mathbf{k}_{3\perp}$ noticeably diminish the magnitude of the cross section. Above the threshold ($k_{2\perp} > k_{th}$) this difference reaches tens per cent while below the threshold the exact cross section is several times smaller than the Born one. It can be explained as follows. Above the threshold the main contribution to the cross section $d\sigma/dx\,d\mathbf{k}_{2\perp}$ is given by the integration region where $\max(\mathbf{k}_{2\perp}^2/\omega_1, \beta_0) \ll \Delta \ll k_{2\perp}$. As a result, the Born cross section is logarithmically amplified as compared to the Coulomb corrections. Far below the threshold where $k_{2\perp} \ll k_{th}$, it follows from the condition $\Delta \ll k_{2\perp}$ that $k_{3\perp} \approx k_{2\perp} \ll m$, and the amplitude is suppressed as a power of $k_{2\perp}^2/m^2$. Therefore, below the threshold the main contribution to the cross section $d\sigma/dx\,d\mathbf{k}_{2\perp}$ is given by the region $k_{3\perp} \sim m$, where the exact in $Z\alpha$ amplitude drastically differs from the Born one. It is seen from Figs.3,4 that in accordance with previous discussion a position of the peak is the same for $x = 0.2$ and $x = 0.8$. Nevertheless, the magnitudes of these two cross sections are significantly different , especially below the threshold. The explanation is the following. For the region $k_{3\perp} \sim m$, which makes the main contribution to the cross section $d\sigma/dx\,d\mathbf{k}_{2\perp}$ below the threshold, and $k_{2\perp} \ll m$ the invariant $s = (k_2 + k_3)^2 \sim m^2 x/(1-x)$. So, $s \ll m^2$ at $x \ll 1$ which leads to the suppression of the cross section below the threshold (see Fig. 3). This is not the case for $1 - x \ll 1$ (see Fig. 5). However, the cross section $d\sigma/dx$ for $x = 0.2$ should coincide with that for $x = 0.8$ and this was checked numerically.

Let us consider now the magnitude of the Coulomb corrections to the cross section $d\sigma/dx$ integrated over the transverse momenta of both final photons. The main contribution to this cross section is given by the region where $|\mathbf{k}_{2\perp}|$, $|\mathbf{k}_{3\perp}| \sim m$. The Born contribution to $d\sigma/dx$ contains large logarithm resulting from the integration over small momentum transfer region $\max(\beta_0, m^2/\omega_1) \ll \Delta \ll m$. For $\beta_0 \gg m^2/\omega_1$ the cross section $d\sigma/dx$ is independent of ω_1, while for $\beta_0 \ll m^2/\omega_1$ it slowly grows (as $\ln \omega_1/m$) when ω_1 increases. Since the Coulomb corrections to $d\sigma/dx$ are determined by the region of momentum transfer $\Delta \sim m$, they do not depend on ω_1 for $\omega_1 \gg m$. They also are insensitive to the effect of screening. In Fig. 5 the exact (solid curve) and the Born (dashed curve) cross sections $\sigma_0^{-1} d\sigma/dx$ are plotted as functions of x for $\omega_1/m = 1000$, and $Z = 83$. As it should be, the curves are symmetric with respect to the replacement $x \to 1 - x$. Dotted curve shows the Coulomb corrections taken with the opposite sign. Note that their dependence on x is very weak. If $x \to 0$ or $x \to 1$ then the cross section $d\sigma/dx$ increases rapidly. However, the cross section $d\sigma/dx$ should vanish at $x = 0$ and $x = 1$ due to the gauge invariance of QED. Actually, the cross section $d\sigma/dx$ begins to decrease very close to the x interval end points ($\delta x \sim m^2/\omega_1^2$). Therefore, the contribution from these x-range to the total cross section σ is negligible. In our example ($Z = 83$, $\omega_1/m = 1000$), the exact result for σ is $3.9 \cdot 10^{-4}$b while the Born approximation gives $4.8 \cdot 10^{-4}$b, the difference being 23%.

In Fig. 6 the Coulomb corrections $d\sigma_c/dx$ divided by σ_0 are shown as a function of Z for $x = 0.7$. Since their dependence on x is rather weak (see Fig. 5), this curve allows one to estimate the magnitude of the Coulomb corrections for any x. It can be seen from Fig. 6 that starting from $Z \approx 30$ the dependence of $\sigma_0^{-1} d\sigma_c/dx$ on Z is almost linear and this quantity is not described by its lowest in $Z\alpha$ approximation ($\propto (Z\alpha)^2$), so that higher order terms are important.

Thus, the process of photon splitting can be adequately described only with the Coulomb corrections taken into account. At large Z their contribution is always noticeable, though the magnitude of the effect depends on the type of a cross section, kinematic conditions, and Z. Indeed, the preliminary experimental data on photon splitting [1] correspond to the cross section being tens per cent smaller than that obtained in the Born approximation. Therefore, the exact in $Z\alpha$ cross section will be in better agreement with the experimental data.

References

[1] Sh. Zh. Akhmadaliev et al. in Proceedings of Interntional Conference PHOTON'97 Egmond-aan-Zee, Netherlands, 10-16/05/97 (to be published).

[2] Y.Shima, Phys.Rev. **142**, 944 (1966).

[3] V.Costantini, B.De Tollis and G.Pistoni, Nuovo Cimento **A 2**, 733 (1971).

[4] V.N.Baier, V.M.Katkov, E.A.Kuraev and V.S.Fadin, Phys.Lett. **B 49**, 385 (1974).

[5] A.M.Johannessen, K.J.Mork and I.Øverbø, Phys.Rev. **D 22**, 1051 (1980).

[6] H.-D.Steinhofer, Z.Phys. **C 18**, 139 (1983).

[7] R.N.Lee, A.I.Milstein, and V.M.Strakhovenko, Zh. Éksp. Teor. Fiz. **112**,1921 (1997) [JETP **85**, 1049 (1997)].

[8] R.N.Lee, A.I.Milstein, and V.M.Strakhovenko, Phys.Rev. **A 57**, 2325 (1998).

[9] A.I.Milstein and V.M.Strakhovenko, Phys. Lett **A 95**, 135 (1983); Zh. Éksp. Teor. Fiz. **85**,14 (1983) [JETP **58**, 8 (1983)].

[10] R.N.Lee and A.I.Milstein, Phys. Lett. **A 198**, 217 (1995); Zh. Éksp. Teor. Fiz. **107**, 1393 (1995) [JETP **80**, 777 (1995)].

[11] A.I.Milstein and M.Schumacher, Phys. Rep. **243**, 183 (1994).

[12] R.N.Lee, A.I.Milstein, and V.M.Strakhovenko, Phys.Rev. **A 58**, 1757 (1998).

[13] G.Z.Molière, Naturforsch. **2a**, 133 (1947).

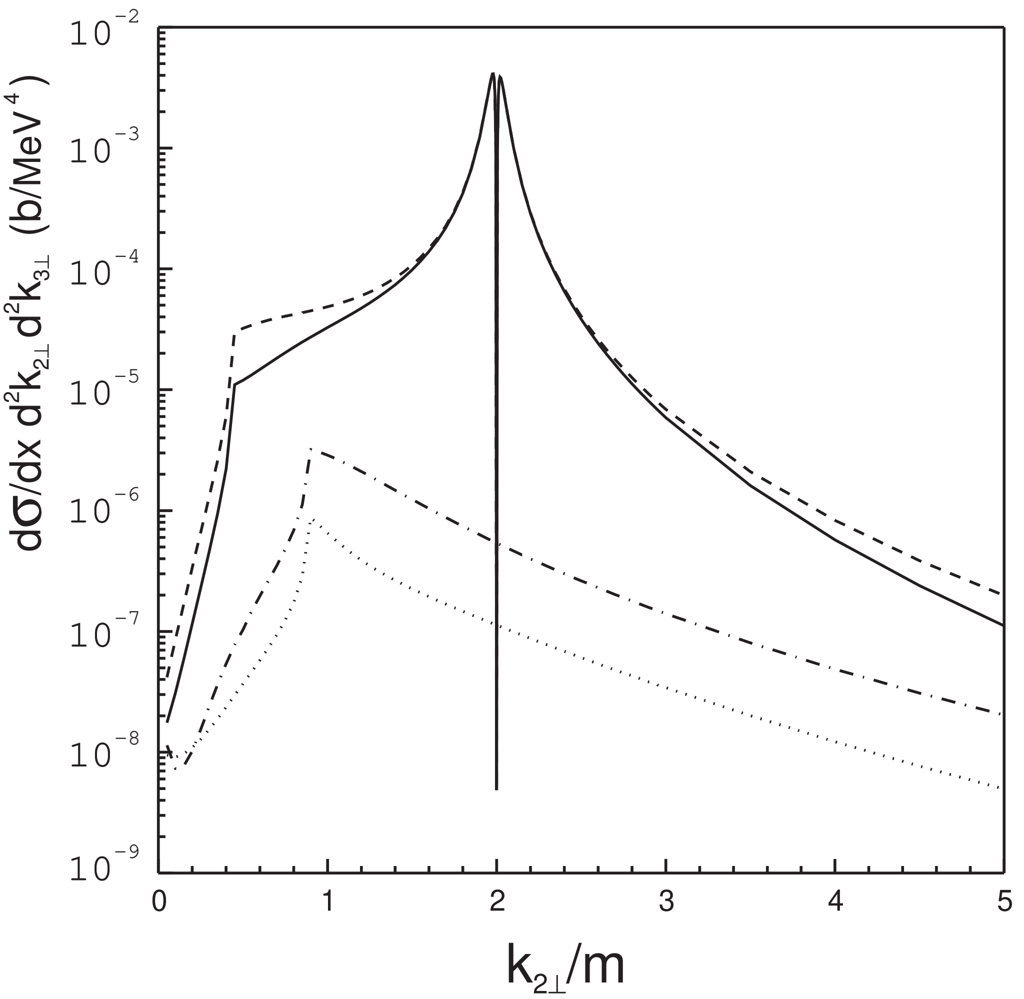

Fig. 1

Figure 1: Differential cross section $d\sigma/dxd\mathbf{k}_{2\perp}d\mathbf{k}_{3\perp}$ vs $|\mathbf{k}_{2\perp}|/m$ in a screened Coulomb potential for different azimuth angle ϕ between vectors $k_{2\perp}$ and $k_{3\perp}$; $Z = 83$, $x = 0.1$, $\omega_1 = 1\text{GeV}$, $k_{3\perp} = 2m$. The dashed curve (Born approximation) and the solid curve (exact cross section) correspond to $\phi = \pi$. The dash-dotted curve (Born approximation) and the dotted curve (exact cross section) correspond to $\phi = 0$.

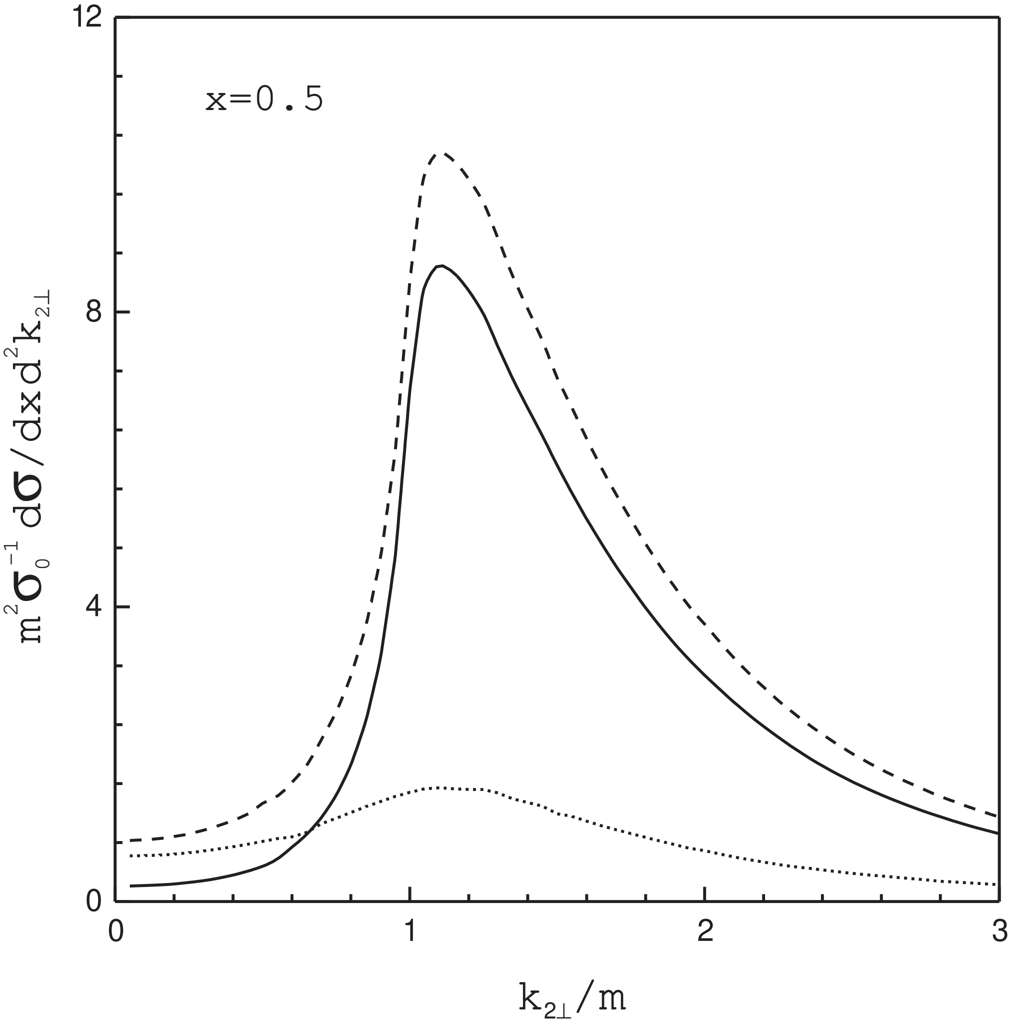

Fig. 2

Figure 2: $m^2\sigma_0^{-1}d\sigma/dxd\mathbf{k}_{2\perp}$ vs $|\mathbf{k}_{2\perp}|/m$ for a screened Coulomb potential, $\omega_1/m = 1000$, $x = 0.5$, $Z = 83$, $\sigma_0 = \alpha^3(Z\alpha)^2/(4\pi^2m^2) = 0.782 \cdot 10^{-9}\,Z^2$ b . The dashed curve corresponds to the Born approximation, the solid curve gives the exact result, and the dotted curve shows the difference between the Born cross section and the exact one.

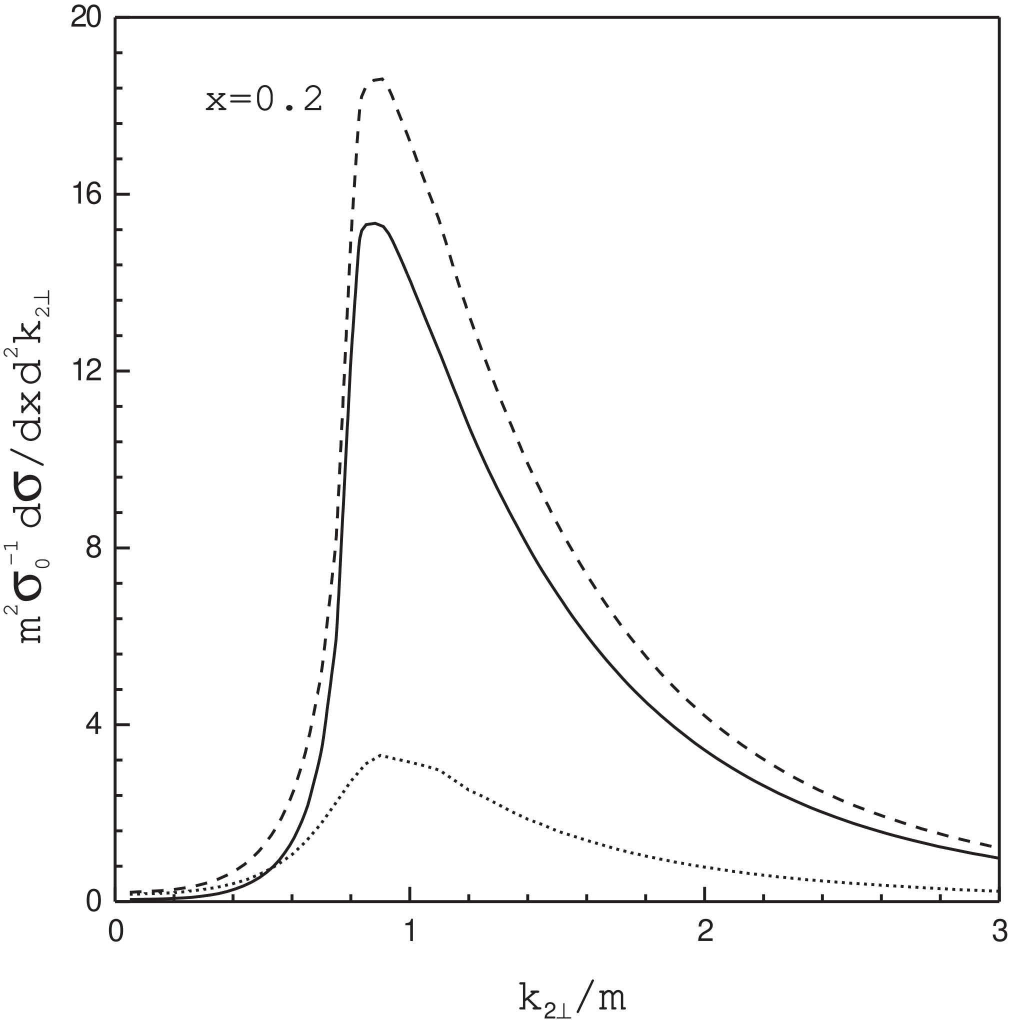

Fig. 3

Figure 3: Same as Fig. 2 but for $x = 0.2$.

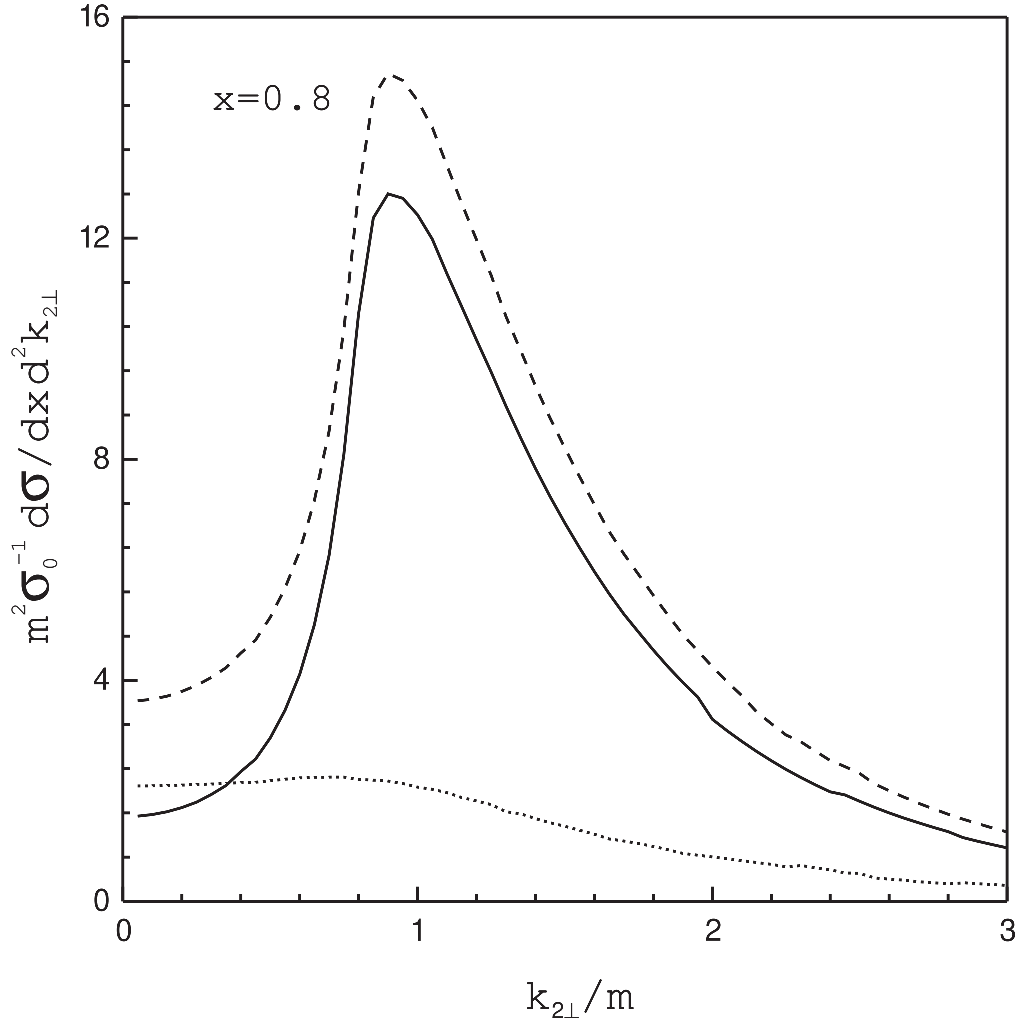

Fig. 4

Figure 4: Same as Fig. 2 but for $x = 0.8$.

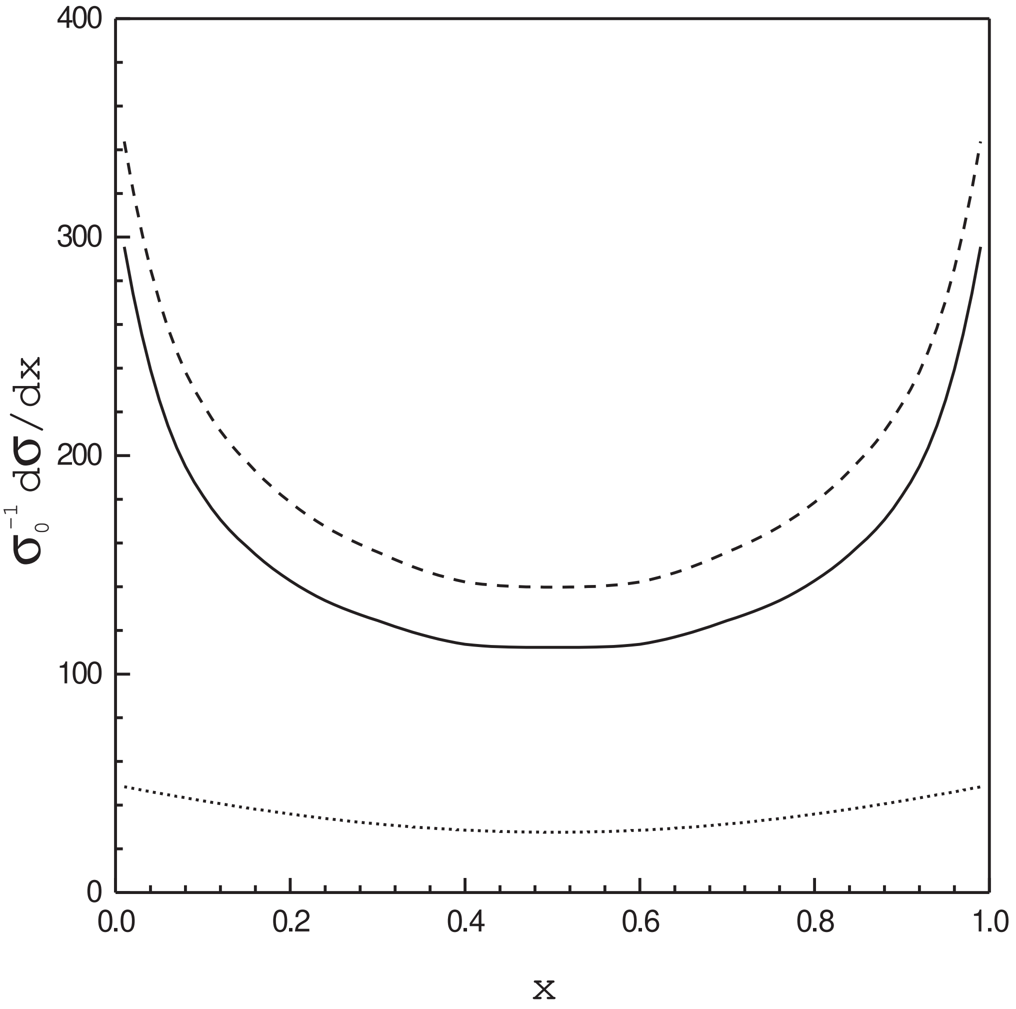

Fig. 5

Figure 5: The dependence of $\sigma_0^{-1} d\sigma/dx$ on x for a screened Coulomb potential, $\omega_1/m = 1000$, $Z = 83$. The dashed curve corresponds to the Born approximation, the solid one gives the exact result, and the dotted curve shows the difference between the Born cross section and the exact one.

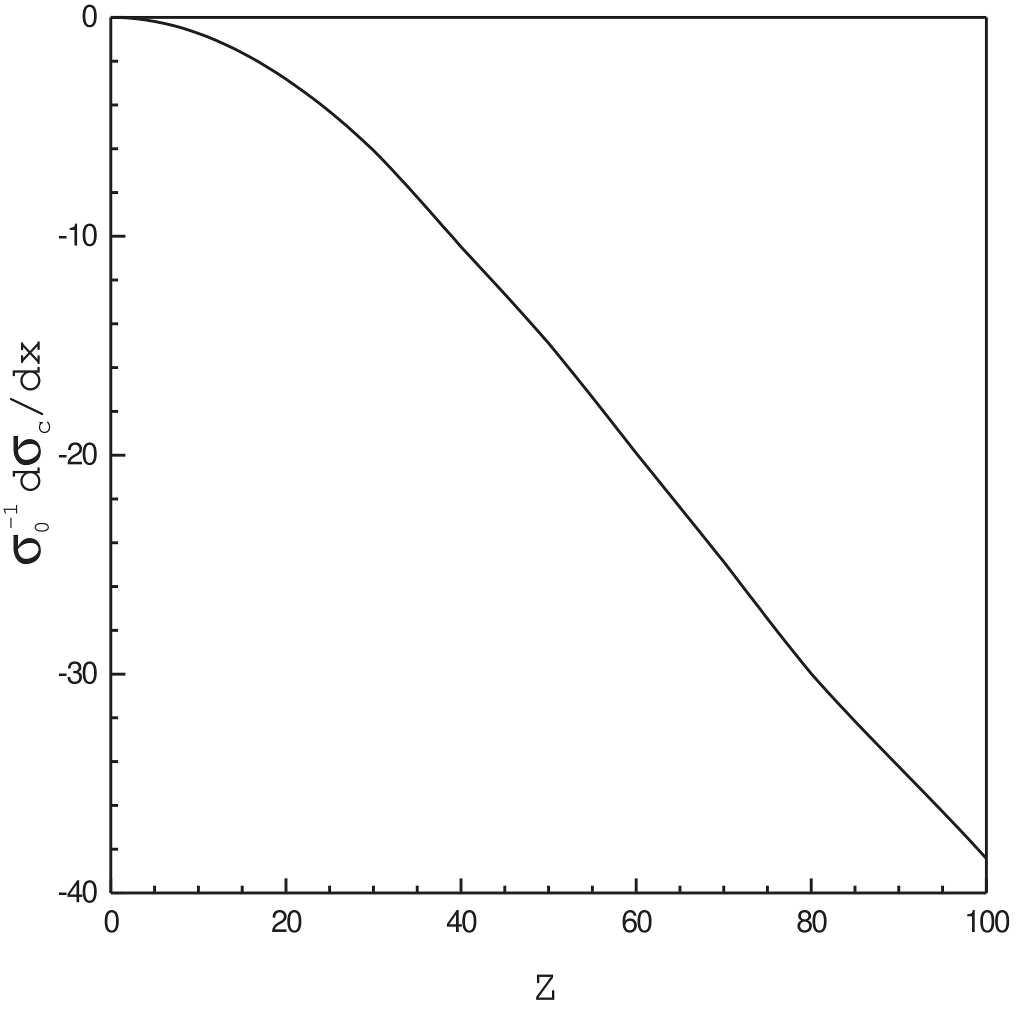

Fig. 6

Figure 6: The dependence of the Coulomb corrections $\sigma_0^{-1} d\sigma_C/dx$ on Z for $x = 0.7$.